JOURNAL OF Applied Polymer SCIENCE

Preparation and Ionic Conductive Properties of All-Solid Polymer Electrolytes Based on Multiarm Star Block Polymers

Shitong Ren,[1] Hefei Chang,[1] Lijuan He,[1] Xiaofei Dang,[2] Yanyan Fang,[3] Liaoyun Zhang,[1*] Huayi Li,[2*] Youliang Hu,[2] Yuan Lin[3]

[1]College of Chemistry and Chemical Engineering, University of Chinese Academy of Sciences, Beijing 100049, People's Republic of China

[2]Joint Laboratory of Polymer Science and Materials, Key Laboratory of Engineering Plastics, Institute of Chemistry, Chinese Academy of Sciences, Beijing 100190, People's Republic of China

[3]Key Laboratory of Photochemistry, Institute of Chemistry, Chinese Academy of Sciences, Beijing 100190, People's Republic of China

Correspondence to: L. Y. Zhang (E-mail: zhangly@ucas.ac.cn); H. Y. Li (E-mail: lihuayi@iccas.ac.cn)

ABSTRACT: A series of star block polymers with a hyperbranched core and 26 arms are successfully synthesized by atom transfer radical polymerization of styrene (St), and poly(ethylene glycol) methyl ether methacrylate from a hyperbranched polystyrene (HBPS) multifunctional initiator. All-solid polymer electrolytes composed of these multiarm star polymers and lithium salts are prepared. The influences of polyoxyethylene (PEO) side-chain length, PEO content, lithium salt concentration and type, and the structure of polymer on ionic conductivity are systematically investigated. The resulting polymer electrolyte with the longest PEO side chains exhibits the best ionic conductive properties. The maximum conductivity is 0.8×10^{-4} S cm^{-1} at 25°C with EO/Li = 30. All the prepared multiarm star block polymers possess good thermal stability. The mechanical property is greatly improved owing to the existence of polystyrene blocks in the multiarm star polymer molecules, and flexible films can be obtained by solution-casting technique.
 J. Appl. Polym. Sci. 129: 1131–1142, 2013

KEYWORDS: properties and characterization; electrochemistry; structure–property relations

Received 14 September 2012; accepted 31 October 2012; published online 26 November 2012
DOI: 10.1002/app.38798

INTRODUCTION

Lithium secondary batteries are widely used in portable, entertainment, computing, and telecommunication equipment because of their advantages of high-energy density, long lifespan, design flexibility, high operational voltage, and no memory effects compared with comparable batteries. However, organic liquid electrolytes are now commonly used in lithium secondary batteries, which have the possibility of leakage and explosion during the process of using and storage. As a result, safety becomes one of the most critical problems of liquid-based lithium secondary batteries. Solid polymer electrolytes (SPEs) composed of polymers and lithium salts contain no organic liquid, and therefore are more secure and reliable. Besides, SPE-based lithium secondary batteries possess lighter weight, higher-energy density, more flexible design than liquid-based lithium secondary batteries, which can better meet the demand of consumers for thinner, lighter, more space-effective and shape-flexible electronic devices.[1–3]

Until now, a large amount of research on the polyoxyethylene (PEO)-based polymer electrolytes has been carried out, and great progresses have been made.[4–14] However, SPEs based on linear PEO with high molecular weight have a high degree of crystallinity, which hinders the transport of ions. Low ionic conductivity (around 10^{-7} S cm^{-1}) is observed at room temperature. This is far from the application requirement of a value above 10^{-3} S cm^{-1} for lithium secondary batteries. To improve the ionic conductivity, random copolymers,[15–17] graft copolymers,[18,19] block copolymers,[20,21] comb polymers,[22–24] and hyperbranched polymers[25–27] based on PEO have been designed to suppress the formation of crystal and, therefore, the ionic conductivity of SPEs based on these polymers was greatly improved.

Star polymers with branched and three-dimensional spherical structure exhibit unique properties and behaviors compared with linear analogues. Their structures are more stable toward the change of external environment because of the connection of covalent bonds between core and arms. In addition, the branched structure of star polymer can inhibit the formation of crystal. Based on these characteristics, a large number of PEO-based star polymers were synthesized and used for polymer electrolytes.[28–31] Ionic conductivity of PEO-based star polymer

electrolytes was significantly higher than PEO-based linear polymer electrolytes because of lower degree of crystallinity, easier motion of PEO chains, and more dissolved salts. Most reported ionic conductivity of PEO-based star polymer electrolyte is about 10^{-5} S cm^{-1}. However, increased flexibility of polymer chains usually leads to poor mechanical properties. To achieve a balance between conductivity and mechanical properties, star copolymers of PEO with hard polymer segments were also designed,[32,33] and freestanding polymer electrolyte films were produced owing to the introduction of rigid blocks.

In this study, a new type of multiarm star polymer with a hyperbranched polystyrene (HBPS) core and block arms was first designed and synthesized by a relatively simple process. HBPS containing chlorine atoms was prepared by atom transfer radical self-condensing vinyl polymerization (ATR-SCVP) of styrene (St) and *p*-chloromethylstyrene (CMS), and the number of chlorine atoms in each HBPS molecule is tunable by changing feed ratios. Star polymers with PS-*b*-PPEGMA block arms were synthesized by atom transfer radical polymerization (ATRP) of styrene (St) and poly(ethylene glycol) methyl ether methacrylate (PEGMA) from HBPS multifunctional initiator. The inner hard PS blocks of the resulting star block polymers are good for improving the mechanical property, whereas the outer PPEGMA block with PEO side chains is in favor of obtaining high conductivity. The influences of PEO side-chain length, PEO content, lithium salt concentration and type on the ionic conductivity of polymer electrolytes based on these prepared star block polymers were studied. Besides, the ionic conductivity of polymer electrolytes with different molecular structures was also compared.

EXPERIMENTAL

Materials

Copper(I) chloride (CuCl, 99%, Beijing Yili Fine Chemicals Co., Ltd., China) was used after washing with acetic acid, methanol, and ether, respectively; *N,N,N′,N″,N‴*-pentamethyldiethylenetriamine (PMDETA, 99%, Aladdin, China), chlorobenzene, and toluene were dried with CaH_2 and distilled under reduced pressure before use; CMS (90%, Aldrich, USA) and styrene (St) were distilled from CaH_2 under reduced pressure and subsequently passed through a column of neutral alumina; 2,2-bipyridine (bpy, 99.5%, Sinopharm Chemical Reagent Co., Ltd., China), PEGMA (M_n = 300, 475, and 950, Aldrich, USA), and ethyl α-bromoisobutyrate (EBrIB, 98%, Aladdin, China) were used without further purification; Lithium *bis*(trifluoromethanesulfonimide) (LiTFSI, 99%, Aladdin, China) and lithium perchlorate ($LiClO_4$, 98%, Aladdin, China) were dried under vacuum at 80°C for 24 h before use. Tetrahydrofuran (THF) used to prepare polymer electrolytes was distilled from CaH_2 before use; all other solvents and reagents were used as received.

Synthesis of Polymers

Synthesis of HBPS. HBPS was synthesized according to the previously published literature.[34] In a typical experiment, bpy (0.659 g, 4.2 mmol), CMS (3.0 mL, 21.1 mmol), styrene (2.4 mL, 21.1 mmol), and chlorobenzene (8.0 mL) were added to a dry round-bottomed flask with rubber septum and magnetic stir bar. The solution was degassed by three freeze–pump–thaw cycles. Afterwards CuCl (0.209 g, 2.1 mmol) was added and another freeze–pump–thaw cycle was conducted. The flask was immersed into a preheated oil bath at 120°C. After 4 h, the reaction was cooled to room temperature, opened to air, and diluted with THF. The reaction mixture was passed through a neutral alumina column to remove the copper residues. Subsequently, the solution was concentrated through rotary evaporation and precipitated into methanol, filtered, and dried overnight at 45°C under vacuum. The product was collected as a white solid. Elemental analysis: found: C 79.20, H 6.63, Cl 14.17.

Synthesis of Star Polystyrene HBPS-$(PS)_x$. In a typical experiment, HBPS (0.5 g, 2 mmol of initiating groups), styrene (46 mL, 400 mmol), and chlorobenzene (40 mL) were added to a dry round-bottomed flask with rubber septum and magnetic stir bar. The solution was degassed by three freeze–pump–thaw cycles. Afterward, CuCl (0.1 g, 1 mmol) was added and another freeze–pump–thaw cycle was conducted. PMDETA (0.21 mL, 1 mmol) was added and the mixture was stirred under nitrogen until it was homogenous. The flask was immersed into a preheated oil bath at 120°C. After 150 min, the reaction was cooled to room temperature, opened to air, and diluted with THF. The reaction mixture was passed through a neutral alumina column to remove the copper residues. Subsequently, the solution was concentrated by rotary evaporation and precipitated into methanol, filtered, and dried overnight at 45°C under vacuum and a white solid was obtained.

Synthesis of Star Block Polymers HBPS-$(PS$-*b*-$PPEGMA)_x$. In a typical experiment, HBPS-$(PS)_x$ (0.5 g, 0.1 mmol of initiating groups), bpy (31.2 mg, 0.2 mmol), PEGMA300 (5.7 mL, 20.0 mmol), and toluene (5 mL) were added to a dry round-bottomed flask with rubber septum and magnetic stir bar. The solution was degassed by three freeze–pump–thaw cycles. Afterward, CuCl (10 mg, 0.1 mmol) was added and another freeze–pump–thaw cycle was conducted. The flask was immersed into a preheated oil bath at 110°C. After desired time, the reaction was cooled to room temperature, opened to air, and diluted with THF. The reaction mixture was passed through a neutral alumina column to remove the copper residues. Subsequently, the solution was concentrated by rotary evaporation and precipitated into hexane for three times, filtered, and dried overnight at room temperature under vacuum. The product was collected as a light yellow solid.

The synthesis of HBPS-$(PS$-*b*-$PEGMA475)_x$ and HBPS-$(PS$-*b*-$PEGMA950)_x$ was similar to the above process. The precipitant for HBPS-$(PS$-*b*-$PEGMA475)_x$ and HBPS-$(PS$-*b*-$PEGMA950)_x$ was ether.

Synthesis of Star Polymer HBPS-$(PPEGMA950)_x$. The procedure was the same as that of the above star block polymers and a general recipe was given as follows: HBPS (0.1 g, 0.4 mmol of initiating groups), bpy (62.5 mg, 0.4 mmol), PEGMA950 (5.0 g, 5.26 mmol), CuCl (19.8 mg, 0.2 mmol), and toluene (5 mL). The reaction was carried out at 110°C for 8 h.

Synthesis of Block Polymer PS-*b*-PPEGMA950. Block polymer PS-*b*-PPEGMA950 was synthesized according to the previously published literature.[35]

Synthesis of PPEGMA950. The procedure was the same as that of the above star block polymers and a general recipe was given as follows: EBrIB (20.0 mg, 0.1 mmol), PEGMA950 (4.75 g, 5 mmol), bpy (31.2 mg, 0.2 mmol), CuBr (14.4 mg, 0.1 mmol), and toluene (5 mL). The reaction was carried out at 80°C for 8 h.

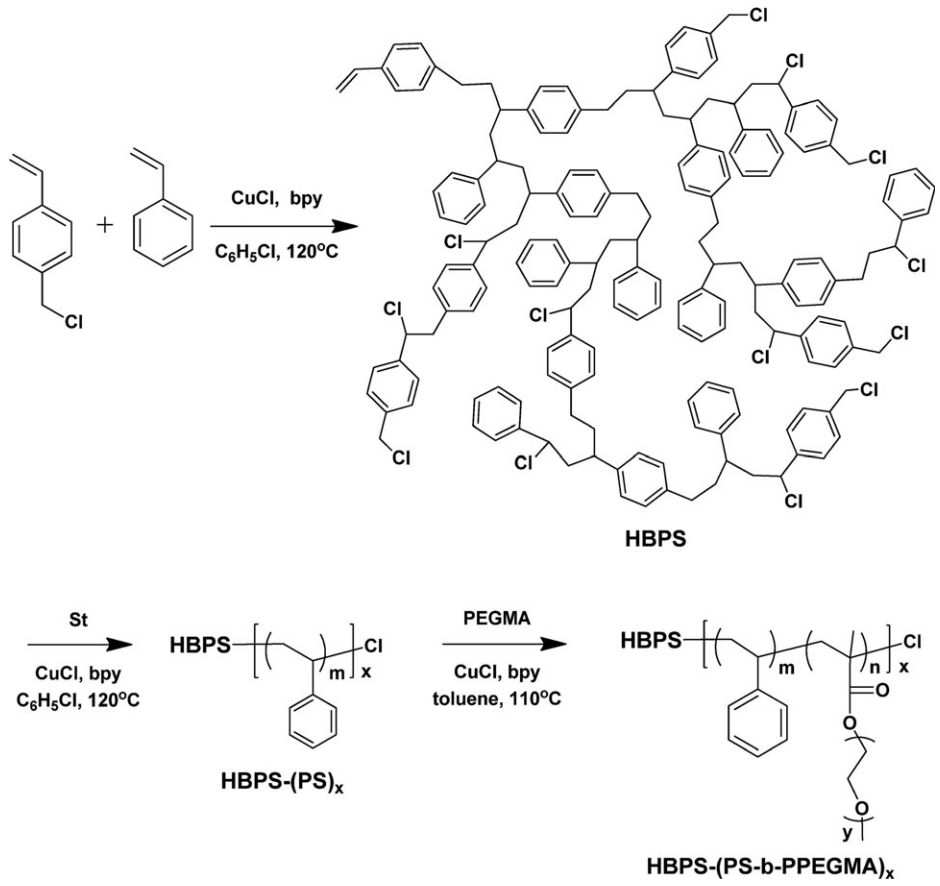

Scheme 1. Synthesis route of multiarm star block polymer.

Preparation of Polymer Electrolytes

The SPEs with different PEO side-chain lengths (PEGMA300, PEGMA475, and PEGMA950), different PEO contents (40.0, 54.1, 59.6, 69.3, and 74.0% for HBPS-(PS-*b*-PPEGMA950)$_x$) and different EO/Li (molar ratio of EO unit and lithium salt for HBPS-(PS-*b*-PPEGMA950)$_x$ with PEO content of 74.0%) were prepared by a solution-casting technique. First, the above-prepared polymers and lithium salt (LiTFSI or $LiClO_4$) were added to THF, and stirred with high speed to form homogeneous solution. Then, the solution was pored into a Teflon mold and evaporated at room temperature for 12 h. Then, the polymer electrolyte was transferred into a vacuum oven for 24 h at 80°C to remove the residual THF.

Characterizations

Nuclear magnetic resonances (^{1}H NMR and ^{13}C NMR) were recorded on a Bruker Avance 400 spectrometer at room temperature with tetramethylsilane (TMS) as internal standard and deuterochloroform ($CDCl_3$) as solvent. Fourier transform infrared (FTIR) analyses were carried out using the attenuated total reflectance (ATR) method on a Perkin-Elmer system 2000 infrared spectrum analyzer. Gel permeation chromatography (GPC) measurements were performed using a Waters 515 HPLC equipped with a Waters 2414 differential refractometer at room temperature with THF as eluent at a flow rate of 1.0 mL min^{-1}. X-ray diffraction (XRD) measurements were carried out on a Shimadzu-6000 X-ray diffractometer with CuKα radiation at a scanning rate of 5° min^{-1} in the 2θ range of 5–60°. Elemental analysis was determined using an elemental analyzer Carlo Erba 1106. Differential scanning calorimetry (DSC) measurements were carried out on a Q2000 instrument in the temperature range from −90 to 150°C at a heating/cooling rate of 10°C min^{-1} under nitrogen atmosphere. The data were collected on the second heating cycle. Thermogravimetric analysis (TGA) was performed under nitrogen atmosphere on a Perkin-Elmer TGA 7 series instrument from 50 to 600°C at a heating rate of 20°C min^{-1}.

The impedance of the polymer electrolytes was measured by electrochemical impedance spectroscopy using a Solartron SI 1287 electrochemical interface and Solartron 1255B frequency response analyzer, with a frequency range of 1 Hz–1000 kHz, AC amplitude of 10 mV, and a temperature range of 25–80°C. Temperature–conductivity plots were obtained by placing the electrochemical cell in an oven set at measuring temperature. The ionic conductivity was calculated from the following equation:

$$\sigma = l/AR_b$$

Here, σ is the ionic conductivity, l is the distance between the two stainless electrodes, A is the area of the polymer electrolyte contacted with the stainless electrodes, and R_b is the bulk resistance, respectively.

RESULTS AND DISCUSSION

Synthesis of Star Polymers

As shown in Scheme 1, the synthesis of multiarm star block polymer with a hyperbranched core was carried out in three

Table I. Conditions and Results of the Prepared Polymers

Polymers	Feed ratios[a]	Content of PEO[b] (wt %)	M_n[c]	M_w[c]	PDI[c]
HBPS	1/1/2/10/10	0	6615	19,845	3.00
HBPS-$(PS)_{26}$	1/0.5/0.5/200	0	30,055	51,394	1.71
HBPS-$(PS\text{-}b\text{-}PPEGMA300)_{26}$	1/1/2/200	62.2	57,879	82,188	1.42
HBPS-$(PS\text{-}b\text{-}PPEGMA475)_{26}$	1/1/2/200	60.1	44,729	76,487	1.71
HBPS-$(PS\text{-}b\text{-}PPEGMA950)_{26}$	1/2/4/60	59.6	43,100	61,202	1.42

[a]Molar ratio of initiating sites/Cu(I)/ligand/monomer, ligand for HBPS-$(PS)_{26}$ is PMDETA, ligand for HBPS, and HBPS-$(PS\text{-}b\text{-}PPEGMA)_{26}$ is 2,2-bipyridine, [b]Calculated from ^{1}H-NMR, [c]Measured by GPC.

steps: (a), HBPS was prepared by ATR-SCVP of *p*-chloromethylstyrene (CMS) and styrene (St); (b), HBPS containing chlorine atoms was used as core to initiate the ATRP of St to prepare multiarm star polystyrene HBPS-$(PS)_x$; (c), HBPS-$(PS)_x$ was used as macroinitiator to further initiate the ATRP of PEGMA. Finally, multiarm star block polymers HBPS-$(PS\text{-}b\text{-}PPEGMA)_x$ were prepared.

The content of Cl in HBPS could be adjusted by changing the feed ratios of CMS and St as reported by the previously published literature.[34] CMS provides the Cl atoms in HBPS which produce arms in the next ATRP reaction. As a result, star polymers with different number of arms can be prepared from HBPS. In our research, HBPS was synthesized with CMS/St = 1/1. Excessive Cl atoms in HBPS make the growth of arms difficult because of large steric hindrance, whereas insufficiency of Cl atoms leads to few arms. Therefore, appropriate CMS/St is needed to make a compromise between the number of arms and the steric hindrance.

The experiment conditions and results of prepared polymers are summarized in Table I. CuCl was used as a catalyst in the preparation of star polymers. PMDETA was the ligand for the synthesis of HBPS-$(PS)_{26}$. Bpy was the ligand for the synthesis of HBPS-$(PS\text{-}b\text{-}PPEGMA)_{26}$ from HBPS-$(PS)_{26}$. The star block polymers were synthesized from the same HBPS-$(PS)_{26}$. As a result, products with the same length of PS blocks and different length of PPEGMA blocks were obtained by changing the feed ratio and reaction time of PEGMA. The content of PEO in the prepared star polymers was calculated from the proton signals of benzene ring and $CH_3(OCH_2CH_2)_9-$ of PEGMA in ^{1}H NMR.

As summarized in Table I, the M_n of HBPS-$(PS)_{26}$ was significantly higher than that of HBPS, indicating that HBPS initiated the ATRP of St. Besides, the higher M_n of HBPS-$(PS\text{-}b\text{-}PPEGMA)_{26}$ than HBPS-$(PS)_{26}$ proved the reaction of PEGMA and HBPS-$(PS)_{26}$. No proton signals of —CHCl— or —CH_2Cl of HBPS and HBPS-$(PS)_{26}$ were observed in ^{1}H NMR (Figures 2 and 3), indicating completely reaction of Cl-initiating sites. Therefore, the number of arms of the obtained star polymers was equal to the number of Cl in HBPS. In total, 26 Cl atoms calculated from M_n and element analysis were contained for each HBPS molecule. As a result, the obtained star polymers were believed to possess 26 arms on average.

Structural Characterization of Polymers

The ^{1}H NMR spectrum of HBPS is shown in Figure 1. The peaks were attributed as follows: 6.42–7.40 (—C_6H_5, —C_6H_4—), 5.67, 5.17 (CH_2=CH—), 4.80 (—CHCl—), and 4.55 (—CH_2Cl). The appearance of peaks at 4.80 and 4.55 proved the branched structure of the obtained HBPS. The degree of branching was 0.22, which was calculated from the proton signals of —CHCl— and —CH_2Cl according to the previously published literature.[34]

^{1}H NMR spectrum of HBPS-$(PS)_{26}$ is shown in Figure 2. No proton signals of —CHCl— (δ = 4.80) and —CH_2Cl (δ = 4.55) of HBPS were observed, indicating the completely reaction of

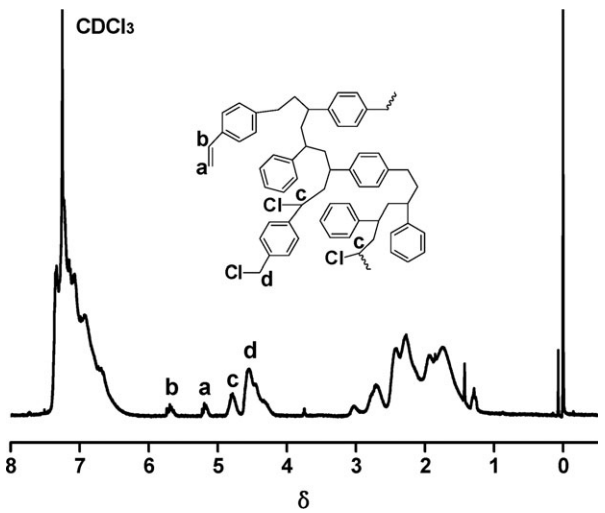

Figure 1. ^{1}H NMR spectrum of HBPS.

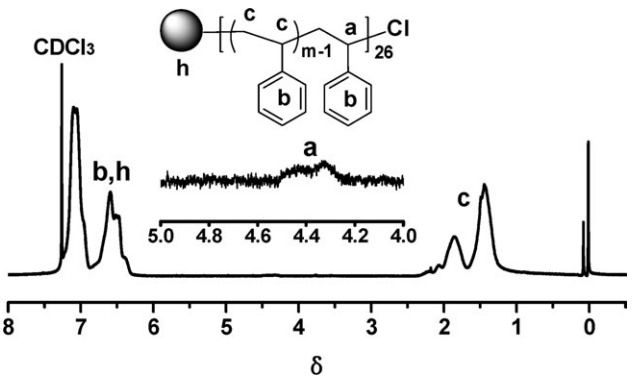

Figure 2. ^{1}H NMR spectrum of HBPS-$(PS)_{26}$.

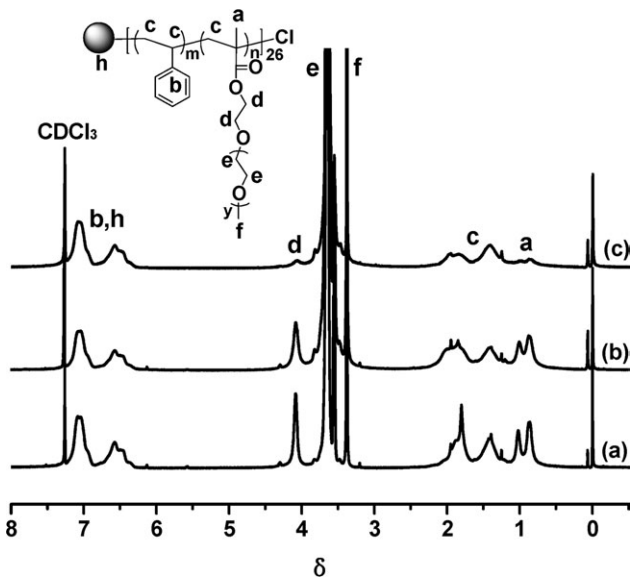

Figure 3. ^{1}H NMR spectra of HBPS-(PS-*b*-PPEGMA)$_{26}$ prepared from PEGMA with different molecular weights (a) PEGMA300, (b) PEGMA475, and (c) PEGMA950.

the initiating sites in HBPS. The peaks at 4.5–4.2 were the proton signals of —CHCl— at the end of each PS arm.

^{1}H NMR spectra of HBPS-(PS-*b*-PPEGMA)$_{26}$ with similar content of PEO (∼ 60 wt %) prepared from PEGMA with different molecular weight are shown in Figure 3. The characteristic peaks corresponding to St repeating units in the PS segments and PEGMA repeating units in the PPEGMA segments were clearly observed. The peaks at 7.2–6.2 and 4.2–3.1 were attributed to the characteristic absorption of the protons of benzyl rings in St units and $CH_3(OCH_2CH_2)_9-$ in PEGMA units, respectively. Besides, the disappearance of the proton signals of —CHCl— (δ = 4.2–4.5) at the end of each PS arm proved that

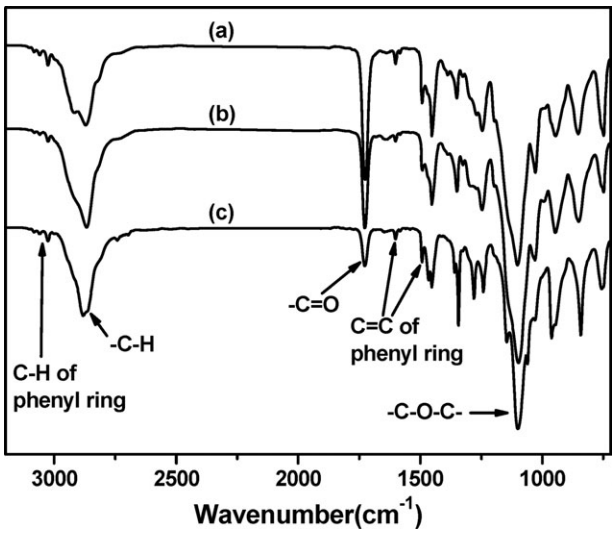

Figure 4. ATR-FTIR spectra of HBPS-(PS-*b*-PPEGMA)$_{26}$ prepared from PEGMA with different molecular weights (a) PEGMA300, (b) PEGMA475, and (c) PEGMA950.

the initiating sites in HBPS-(PS)$_{26}$ initiated the ATRP of PEGMA.

ATR-FTIR spectra of HBPS-(PS-*b*-PPEGMA)$_{26}$ with similar content of PEO (∼ 60 wt %) prepared from PEGMA with different molecular weights are shown in Figure 4. The appearance of peaks at 3100–3000, 1601, and 1492 cm^{-1} indicated the existence of St units. The peaks at 1730 and 1100 cm^{-1} were attributed to the —C=O stretching vibration absorption and —C—O—C— stretching vibration absorption of PEGMA units, respectively.

The results of ^{1}H NMR, ATR-FTIR spectra, and the change of molecular weight compared with HBPS-(PS)$_{26}$ indicated that HBPS-(PS-*b*-PPEGMA)$_{26}$ was successfully synthesized.

Star polymer HBPS-(PPEGMA)$_{26}$ was also synthesized from HBPS, without the blocks of PS. Figure 5 shows the ^{1}H NMR spectrum of HBPS-(PPEGMA)$_{26}$. Both of the peaks corresponding to HBPS core (δ = 7.4–6.6) and PPEGMA arms (δ = 4.2–3.1, 1.1–0.7) appeared. Because of the growth of PPEGMA arms, the intensity of peak at 7.4–6.6 belonging to proton absorption of benzyl ring in HBPS core was weak. In addition, the signals of —CHCl— and —CH_2Cl in HBPS disappeared, which proved the successful synthesis of HBPS-(PPEGMA)$_{26}$.

Ionic Conductivity

The Effect of the Length of PEO Chain on Ionic Conductivity. PEGMA possesses a reactive vinyl group and a flexible short PEO chain. Polymers based on PEGMA have been widely used for polymer electrolyte matrix.[22–24] Wang et al.[36] studied the influence of the different PEO chain length on PPEGMA-based polymer electrolytes and a positive relationship between ionic conductivity and PEO length was observed. Niitani et al.[37] reported the impact of different PEO chain length on block copolymer PS-*b*-PPEGMA-*b*-PS and the results showed that the length of PEO had no significant effect on ionic conductivity. To explore the effect of the PEO side-chain length of the star block polymers on ionic conductivity, three PEGMA with different molecular weights including PEGMA300

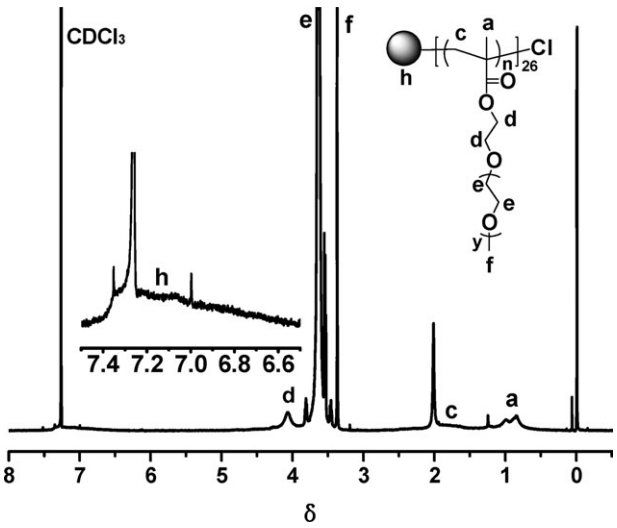

Figure 5. ^{1}H NMR spectrum of HBPS-(PPEGMA950)$_{26}$.

Applied Polymer SCIENCE

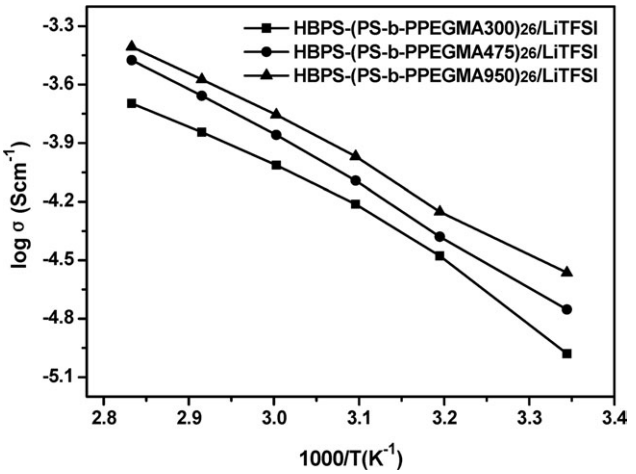

Figure 6. The temperature dependence of ionic conductivity of HBPS-(PS-*b*-PPEGMA)$_{26}$/LiTFSI with different PEO side-chain lengths.

(4.5 EO groups), PEGMA475 (8.5 EO groups), and PEGMA950 (19.3 EO groups) were used as monomers. Star block copolymers HBPS-(PS-*b*-PPEGMA)$_{26}$ with different lengths of PEO chains and similar content of PEO were synthesized. Corresponding polymer electrolytes were prepared with LiTFSI as lithium salt.

Figure 6 shows the temperature dependence of ionic conductivity of HBPS-(PS-*b*-PPEGMA)$_{26}$/LiTFSI with different PEO side-chain lengths. The three polymer electrolytes had similar PEO content ($\sim$ 60 wt %) and the same content of lithium salt (EO/Li = 20). It was obvious that the ionic conductivity of the three polymer electrolytes based on HBPS-(PS-*b*-PPEGMA)$_{26}$ gradually increased with the increase of the length of PEO side chains. Polymer electrolyte with the longest PEO side chains (19.3 EO units) exhibited the highest ionic conductivity. This was explained by the larger free volume resulted from the intertwining of the PEO side chains,[35] which facilitated the motion of ions in the polymer matrix.

DSC curves of the star block polymers with different lengths of PEO side chains and their corresponding polymer electrolytes are shown in Figure 7. No melting peak owing to crystallization was observed for star polymers containing PEGMA300 or PEGMA475 units except for glass transition, whereas an obvious melting peak appeared with a melting temperature (T_m) of 37.8°C for star polymer containing PEGMA950 units. The above results indicated that HBPS-(PS-*b*-PPEGMA300)$_{26}$ and HBPS-(PS-*b*-PPEGMA475)$_{26}$ were amorphous polymers but HBPS-(PS-*b*-PPEGMA950)$_{26}$ was crystalline polymer. After doping of LiTFSI, melting peak of HBPS-(PS-*b*-PPEGMA950)$_{26}$ disappeared and an apparent glass transition was observed (T_g = −49.1°C). This was because the coordination between lithium salt and EO units disturbed the ordered structure of PEO chains. For HBPS-(PS-*b*-PPEGMA300)$_{26}$ and HBPS-(PS-*b*-PPEGMA475)$_{26}$, T_g was significantly increased when lithium salt was added. This change was also caused by the coordination between lithium salt and EO units, which hindered the motion of the PEO chains. Besides, T_g of the polymer electrolytes deceased with increasing the length of PEO side chains. Therefore, the increase of the PEO side-chain length was good for the improvement of ionic conductivity.

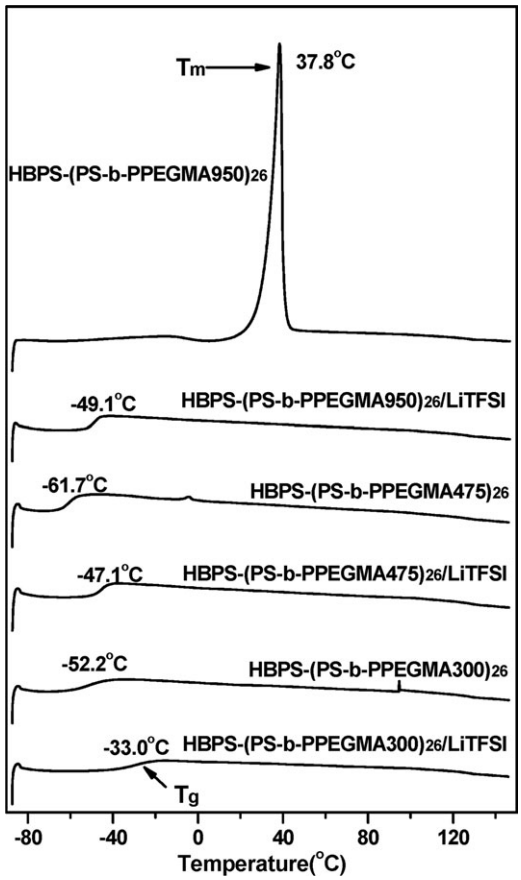

Figure 7. DSC curves of HBPS-(PS-*b*-PPEGMA)$_{26}$ with different lengths of PEO side chain and their corresponding polymer electrolytes.

Figure 8 shows the XRD patterns of HBPS-(PS-*b*-PPEGMA)$_{26}$ with different PEO side-chain lengths and HBPS-(PS-*b*-PPEGMA950)$_{26}$/LiTFSI (EO/Li = 20). Only one broad diffraction peak appeared in the XRD patterns of HBPS-

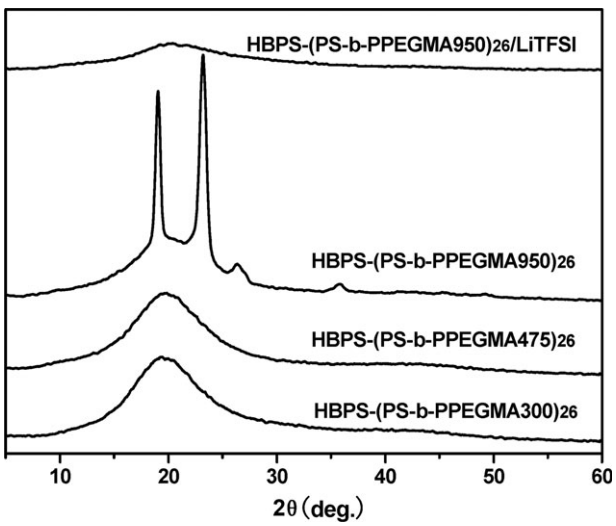

Figure 8. XRD patterns of HBPS-(PS-*b*-PPEGMA)$_{26}$ with different lengths of PEO side chain and HBPS-(PS-*b*-PPEGMA950)$_{26}$/LiTFSI (EO/Li = 20).

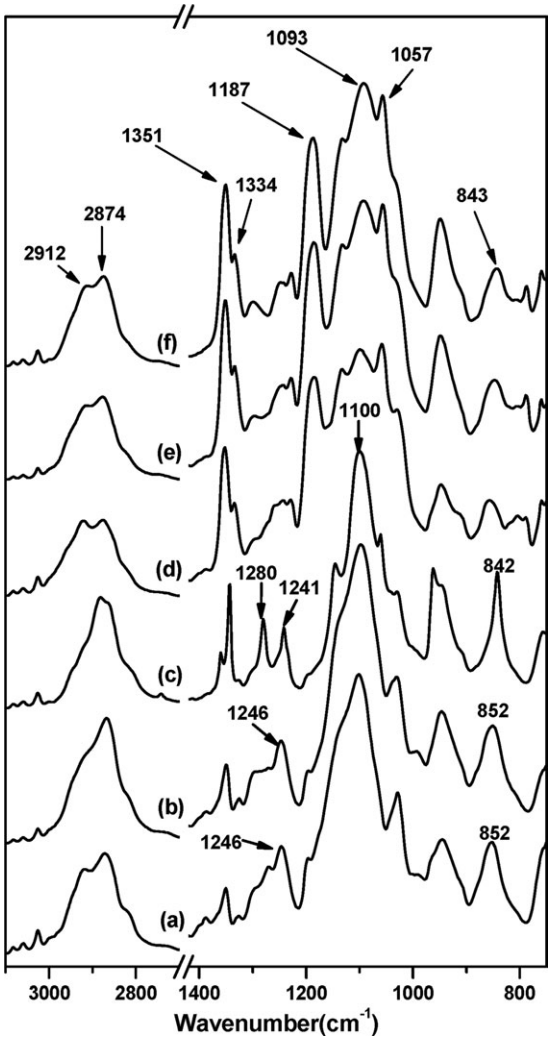

Figure 9. ATR-FTIR spectra of (a) HBPS-(PS-*b*-PPEGMA300)$_{26}$, (b) HBPS-(PS-*b*-PPEGMA475)$_{26}$, (c) HBPS-(PS-*b*-PPEGMA950)$_{26}$, (d) HBPS-(PS-*b*-PPEGMA300)$_{26}$/LiTFSI, (e) HBPS-(PS-*b*-PPEGMA475)$_{26}$/LiTFSI, and (f) HBPS-(PS-*b*-PPEGMA950)$_{26}$/LiTFSI.

(PS-*b*-PPEGMA300)$_{26}$ and HBPS-(PS-*b*-PPEGMA475)$_{26}$. Two strong peaks at about 19 and 23° appeared in the XRD pattern for HBPS-(PS-*b*-PPEGMA950)$_{26}$, indicating semicrystalline nature of the polymer. After the adding of LiTFSI, only a weaker and broader peak was observed, which suggested a significant decrease in PEO crystallinity, resulting from the coordination between the added LiTFSI and the EO units. These results of XRD were completely consistent with the results of DSC.

FTIR is a powerful tool to study the existence state of salt in polymer electrolyte and the interaction between salt and polymer matrix. Figure 9 shows the ATR-FTIR spectra of the star block polymers with different lengths of PEO side chains and their electrolytes. The above DSC and XRD results showed that HBPS-(PS-*b*-PPEGMA300)$_{26}$ and HBPS-(PS-*b*-PPEGMA475)$_{26}$ were amorphous polymers, and HBPS-(PS-*b*-PPEGMA950)$_{26}$ was crystalline polymer. Comparing the FTIR spectra of the three polymers, differences appeared in the following regions: (a) wavenumbers around 2900 cm^{-1} (symmetric and antisymmetric C—H stretching bands); (b) wavenumbers around 1200–1300 cm^{-1} (CH_2 twisting band); (c) wavenumbers around 850 cm^{-1} (CH_2 rocking band). As these three polymers had the same structure but different lengths of the PEO side chains, the above differences were related to the existence of the crystalline regions. After doping of lithium salt, changes around 2900, 1300–1200, and 850 cm^{-1} were also observed for HBPS-(PS-*b*-PPEGMA300)$_{26}$ and HBPS-(PS-*b*-PPEGMA475)$_{26}$, indicating that those differences were caused by the interaction between lithium salt and PEO chains. Besides, the above three regions were all significantly changed after adding LiTFSI for HBPS-(PS-*b*-PPEGMA950)$_{26}$, and a spectrum similar to polymer electrolytes based on HBPS-(PS-*b*-PPEGMA300)$_{26}$ and HBPS-(PS-*b*-PPEGMA475)$_{26}$ was observed. This indicated that the crystalline structure of HBPS-(PS-*b*-PPEGMA950)$_{26}$ was destroyed, which was consistent with the DSC and XRD results. From the above discussion, it was concluded that signals nearby 2900, 1200–1300, and 850 cm^{-1} were not related only to the existence of crystalline phase, but also the interaction between the polymer matrix with lithium salt. In addition, peak around 1100 cm^{-1} corresponding to asymmetric —C—O—C— stretching moved toward lower wavenumbers after doping of lithium salt because of the interaction between EO units and salt. According to the literature reports,[38,39] the peak at 1351 cm^{-1} was attributed to the asymmetric SO_2 stretching of TFSI^{-1}-free ions, and the shoulder peak at lower wavenumber was related to ion pairs or ion aggregation, indicating that LiTFSI was dissociated but not completely.

The Effect of PEO Content on Ionic Conductivity. According to the above result that the prepared polymer electrolyte with the longest PEO side chains had the highest ionic conductivity, HBPS-(PS-*b*-PPEGMA950)$_{26}$/LiTFSI with different contents of PEO and the same EO/Li (20/1) were prepared to study the effect of the content of PEO on ionic conductivity. Figure 10 shows the temperature dependence of ionic conductivity for HBPS-(PS-*b*-PPEGMA950)$_{26}$/LiTFSI with different PEO contents. A positive relationship between PEO content and ionic conductivity was clearly observed. With the increase of PEO

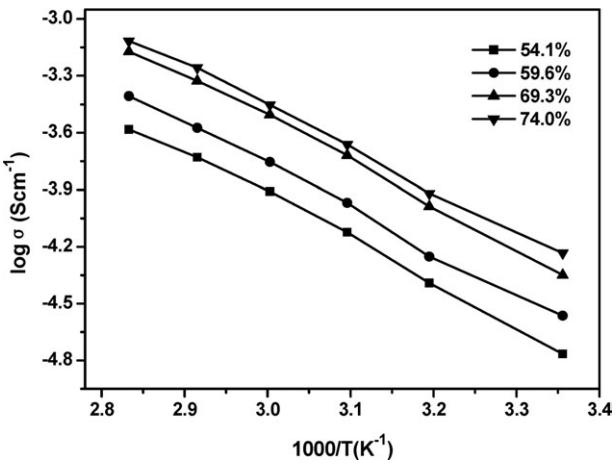

Figure 10. The temperature dependence of ionic conductivity of HBPS-(PS-*b*-PPEGMA950)$_{26}$/LiTFSI with different contents of PEO.

Applied Polymer SCIENCE

Table II. T_g, T_m, and ΔH_m of HBPS-(PS-*b*-PPEGMA950)$_{26}$ with Different PEO Contents and Their Corresponding Polymer Electrolytes

Polymers/polymer electrolytes	Content of PEO (wt %)	T_g (°C)	T_m (°C)	ΔH_m (J g^{-1})
HBPS-(PS-*b*-PPEGMA950)$_{26}$	54.1	–	34.3	40.7
	59.6	–	37.8	54.2
	69.3	–	38.6	66.3
	74.0	–	38.7	84.1
HBPS-(PS-*b*-PPEGMA950)$_{26}$/ LiTFSI (EO/Li = 20/1)	54.1	−48.3	–	–
	59.6	−49.1	–	–
	69.3	−50.3	–	–
	74.0	−51.6	–	–

content, more free ions were produced with the same EO/Li and the content of PS in the polymer electrolytes reduced accordingly. More carriers and small hindrance of PS led to the increase of ionic conductivity.

The T_g, T_m, and ΔH_m of HBPS-(PS-*b*-PPEGMA950)$_{26}$ with different PEO contents and their corresponding polymer electrolytes are summarized in Table II. T_m of all the star block polymers was not greatly affected by the PEO content, but the ΔH_m increased significantly because of the increase of PEO crystalline regions. After doping of lithium salt (EO/Li = 20), no melting peak was observed for all the polymers electrolytes except for glass transition, indicating completely amorphous of the prepared polymer electrolytes. T_g of these polymer electrolytes decreased with increasing PEO content. This was also one of the reasons for the change of ionic conductivity by adjusting PEO content.

The relationship of the ionic conductivity of the star polymer electrolytes and the PEO content at different temperature is shown in Figure 11. With the increase of PEO content, the increase of ionic conductivity at high PEO content was more obvious than that at low PEO content, which became more evident at higher temperature. This may be caused by the structures of the star block polymer. For HBPS-(PS-*b*-PPEGMA950)$_{26}$, the PPEGMA950 blocks grew with the increase of PEO content. Outer PEO chains had smaller steric hindrance and therefore were easier to move. The longer the PPEGMA950 block was, the smaller steric hindrance the outer PEO chains had, and the faster the ionic conductivity increased.

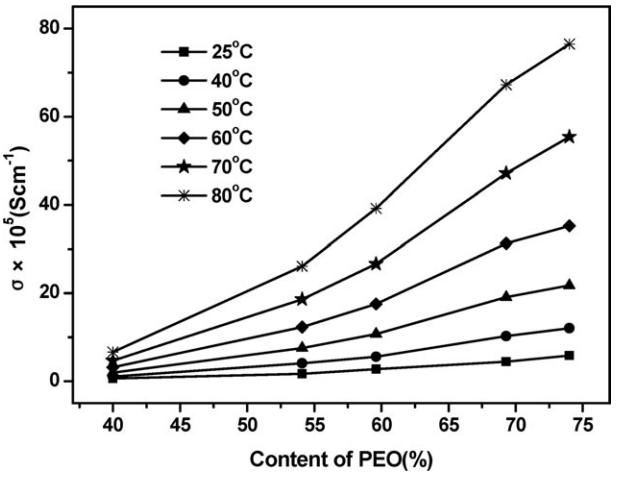

Figure 11. The relationship of the ionic conductivity and the PEO content at different temperatures.

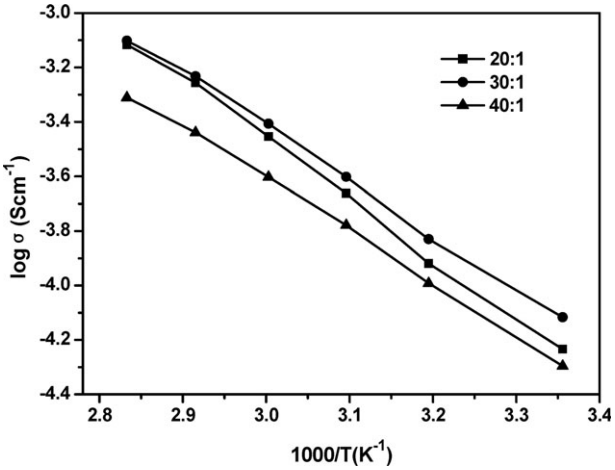

Figure 12. The temperature dependence of ionic conductivity of HBPS-(PS-*b*-PPEGMA950)$_{26}$/LiTFSI with different EO/Li.

The Effect of Lithium Salt Content on Ionic Conductivity. Figure 12 shows the temperature dependence of ionic conductivity of HBPS-(PS-*b*-PPEGMA950)$_{26}$/LiTFSI with different EO/Li. In the testing temperature range, the polymer electrolyte showed the highest ionic conductivity with EO/Li = 30/1. The maximum value at 25°C was 0.8×10^{-4} S cm^{-1}. This was because when the content of lithium salt was low, lithium salt in the polymer matrix was easy to dissociation. With the increase of the lithium salt content, the number of carriers increased and conductivity improved accordingly. When the lithium salt content was increased to a certain extent, ionic conductivity reached a maximum value. Continuing to increase the lithium salt concentration, ion aggregates began to appear, and free ions were replaced by ion aggregates, which reduced the number of carriers and hindered the motion of PEO chains. Therefore, the conductivity of the star polymer electrolytes decreased.

Figure 13 shows the DSC curves of HBPS-(PS-*b*-PPEGMA950)$_{26}$/LiTFSI with different lithium salt contents. T_m and ΔH_m of the polymer electrolyte decreased with increasing lithium salt content, owing to the interaction of the lithium salt and PEO chains. The melting peak disappeared completely at EO/Li = 20. Further increasing the content of lithium salt, T_g gradually increased. This explained the change of ionic conductivity with lithium salt concentration. When the lithium salt content was low, the polymer had a high degree of crystallinity and few carriers. The existence of large amount of crystalline phase hindered the transport of ions. When the lithium salt concentration was high, ion aggregation and physical crosslink made the T_g increased significantly. As a result, the motion of PEO chains became difficult and the ionic conductivity

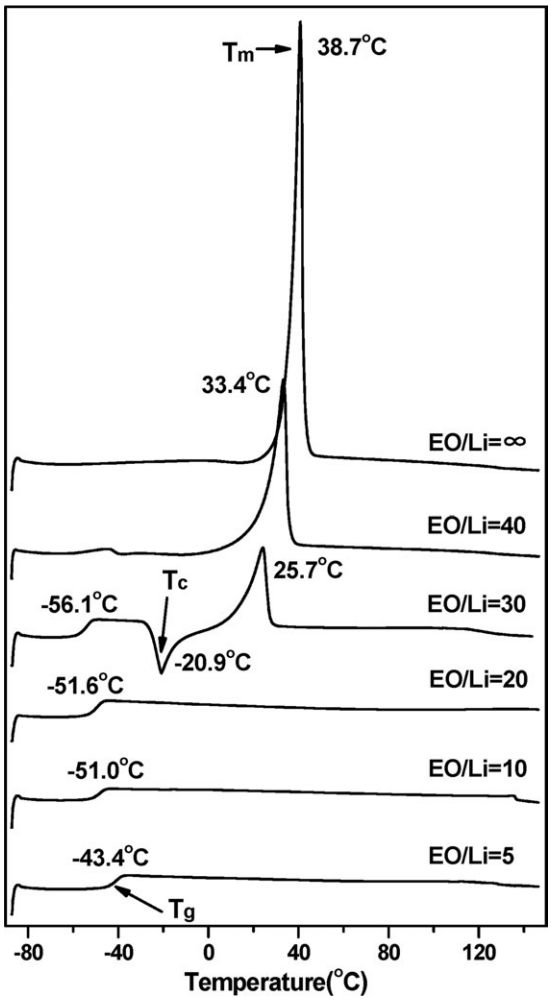

Figure 13. DSC curves of HBPS-(PS-*b*-PPEGMA950)$_{26}$/LiTFSI with different EO/Li.

decreased accordingly. Therefore, the appropriate EO/Li (30/1) was needed to achieve the highest conductivity.

Figure 14 shows the ATR-FTIR spectra of HBPS-(PS-*b*-PPEGMA950)$_{26}$/LiTFSI with different content of LiTFSI. After doping of lithium salt, —C—O—C— absorption peak moved from 1100 cm^{-1} toward lower wavenumbers, which became more obvious with the increase of lithium salt content. The same trend was also observed for changes around 1200–1300 cm^{-1}. The absorption at 1241 and 1280 cm^{-1} gradually disappeared with increasing lithium salt content, indicating that crystallinity deceased with increasing the lithium salt content. The relative intensity of the peak at 1350 cm^{-1} corresponding to the absorption of TFSI^{-1} free ion decreased with the increase of lithium content, compared with the intensity of the shoulder peak at lower wavenumber corresponding to ion pairs or ion aggregates, indicating that ion pairs or ion aggregates gradually increased with the increase of the content of lithium salt. As a result, a maximum ionic conductivity was observed with changing the content of lithium salt.

The Effect of Type of Lithium Salt on Ionic Conductivity. Lithium salt is an important component of polymer electrolyte, which has a significant influence on ionic conductivity of the polymer electrolyte. Figure 15 shows the temperature dependence of ionic conductivity of polymer electrolytes based on HBPS-(PS-*b*-PPEGMA950)$_{26}$ with different lithium salts. The content of PEO was 74.0 wt % and the EO/Li was 30/1. It was obvious that polymer electrolyte with LiTFSI as lithium salt exhibited higher conductivity than polymer electrolyte with $LiClO_4$ as lithium salt in the testing temperature region. This was because LiTFSI was easier to dissociation than $LiClO_4$. More free ions were produced with the same content of lithium. In addition, the large anion TFSI^{-1} played the role of plasticizer, reducing the T_g of the star polymer. An obvious inflection (nearly 40°C) was found for polymer electrolyte with $LiClO_4$, indicating a phase transition happened when raising temperature. These phenomena were explained by the results of DSC of the polymer electrolytes shown in Figure 16. T_g and ΔH_m of HBPS-(PS-*b*-PPEGMA950)$_{26}$/LiTFSI were significantly lower than that of HBPS-(PS-*b*-PPEGMA950)$_{26}$/$LiClO_4$, which facilitated the transport of ions. T_ms for HBPS-(PS-*b*-PPEGMA950)$_{26}$/LiTFSI and HBPS-(PS-*b*-PPEGMA950)$_{26}$/$LiClO_4$ were 25.7 and 33.3°C, respectively. As a result, amount of crystalline phase existed at the temperature below 40°C for

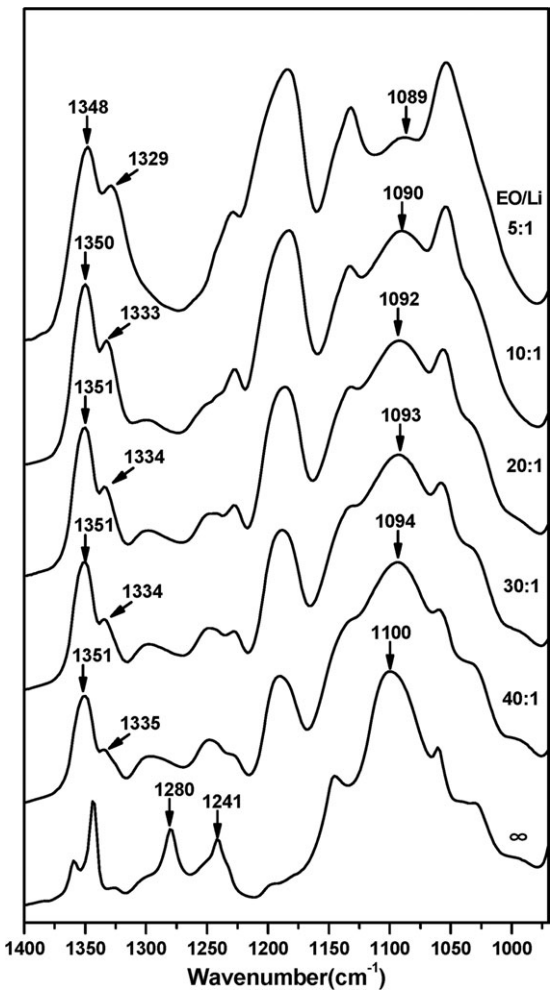

Figure 14. ATR-FTIR spectra of HBPS-(PS-*b*-PPEGMA950)$_{26}$/LiTFSI with different EO/Li.

Applied Polymer SCIENCE

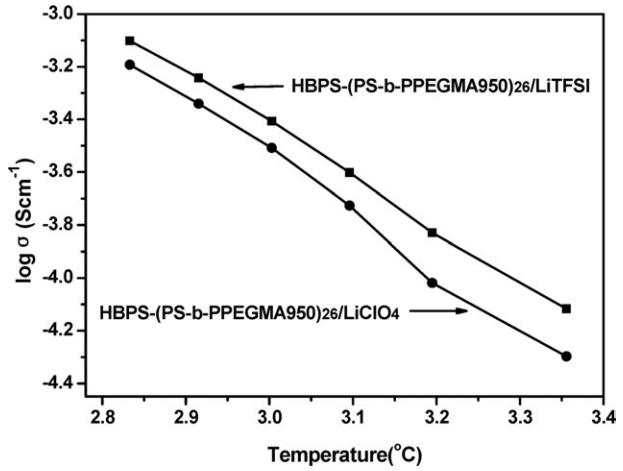

Figure 15. The temperature dependence of ionic conductivity of HBPS-(PS-*b*-PPEGMA950)$_{26}$/LiTFSI and HBPS-(PS-*b*-PPEGMA950)$_{26}$/$LiClO_4$.

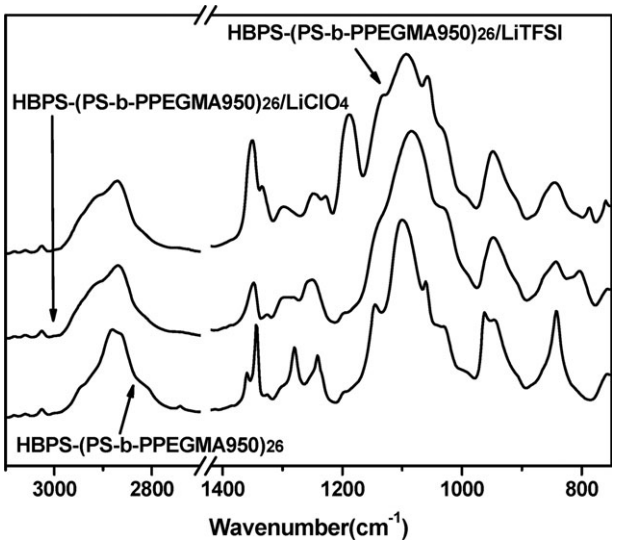

Figure 17. ATR-FTIR spectra of HBPS-(PS-*b*-PPEGMA950)$_{26}$ electrolytes with different lithium salts.

HBPS-(PS-*b*-PPEGMA950)$_{26}$/$LiClO_4$, whereas the crystalline phase disappeared at temperature above 40°C.

Figure 17 shows the ATR-FTIR spectra of the polymer electrolytes prepared with different lithium salts. After doping of lithium salt, the change around 1200–1300 cm^{-1} for HBPS-(PS-*b*-PPEGMA950)$_{26}$/LiTFSI was more obvious than HBPS-(PS-*b*-PPEGMA950)$_{26}$/$LiClO_4$, indicating a more severe interaction between ions and PEO chains and a lower degree of crystallinity, which was consistent with the DSC results.

The Effect of Molecular Structure on Ionic Conductivity. To study the effect of molecular structure on the ionic conductivity of the PPEGMA950-based polymer electrolyte, comb polymer PPEGMA950, block polymer PS-*b*-PPEGMA950, and star polymer HBPS-(PPEGMA950)$_{26}$ were also synthesized to compare with star block polymer HBPS-(PS-*b*-PPEGMA950)$_{26}$. Figure 18 shows the temperature dependence of ionic conductivity of PPEGMA950-based polymer electrolytes with EO/Li = 30. Polymer electrolytes based on PPEGMA950 and HBPS-(PPEGMA950)$_{26}$ exhibited higher conductivity than polymer electrolytes based on HBPS-(PS-*b*-PPEGMA950)$_{26}$ and PS-*b*-PPEGMA950 because of higher content of PEO, but they were sticky liquid at room temperature. Comparing PPEGMA950 and HBPS-(PPEGMA950)$_{26}$ polymer electrolytes, HBPS-(PPEGMA950)$_{26}$ polymer electrolyte had higher ionic conductivity in the testing temperature range. Comparing with the polymer electrolyte based on PS-*b*-PPEGMA950, HBPS-(PS-*b*-PPEGMA950)$_{26}$ polymer electrolyte exhibited higher ionic conductivity in the testing temperature range. The higher ionic conductivity of star polymer electrolytes was attributed to more arms which could have better solubility of lithium salt. According to the above discussion, the ionic conductivity of the prepared star polymers was better than polymer electrolytes based on comb or block polymer.

The results of DSC of polymers with different structures and their corresponding electrolytes are summarized in Table III. It was obvious that PPEGMA950 and HBPS-(PPEGMA950)$_{26}$ had

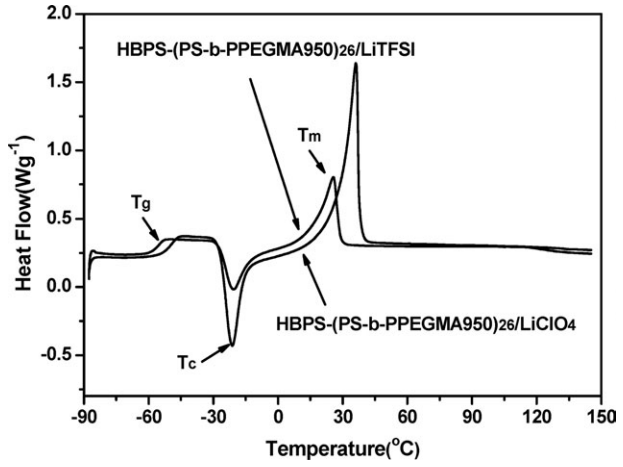

Figure 16. DSC curves of HBPS-(PS-*b*-PPEGMA950)$_{26}$ electrolytes with different lithium salts.

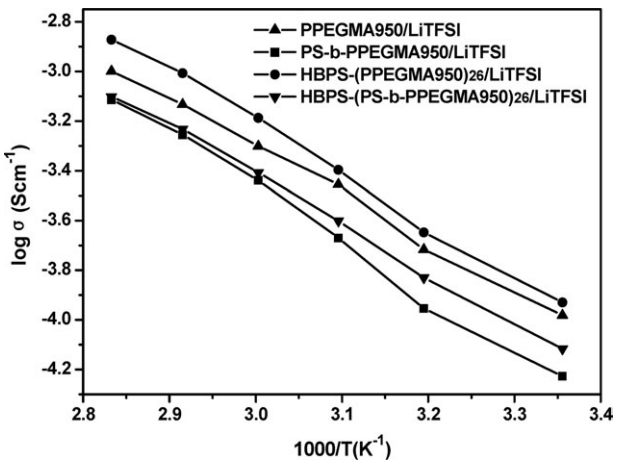

Figure 18. The temperature dependence of ionic conductivity of PPEGMA950-based polymers electrolytes with different structures.

Table III. The DSC Results of Polymers with Different Structures and Their Corresponding Electrolytes

Polymer/polymer electrolyte	EO/Li	T_g (°C)	T_m (°C)	ΔH_m (J g^{-1})
HBPS-(PS-*b*-PPEGMA950)$_{26}$	∞	-	38.7	84.1
PS-*b*-PPEGMA950	∞	-	35.7	105.5
HBPS-(PPEGMA950)$_{26}$	∞	-	37.1	136.3
PPEGMA950	∞	-	36.5	139.8
HBPS-(PS-*b*-PPEGMA950)$_{26}$/LiTFSI	30/1	−52.7	25.7	30.2
PS-*b*-PPEGMA950/LiTFSI	30/1	−52.1	26.1	35.3
HBPS-(PPEGMA950)$_{26}$/LiTFSI	30/1	−52.7	27.0	37.1
PPEGMA950/LiTFSI	30/1	−53.9	32.0	38.5

high ΔH_m because of high content of PEO. But the ΔH_m of PS-*b*-PPEGMA950 was significantly higher than that of HBPS-(PS-*b*-PPEGMA950)$_{26}$ with similar content of PEO, indicating that star structure inhibited the formation of crystal to a certain extent. T_g of HBPS-(PS-*b*-PPEGMA950)$_{26}$/LiTFSI was −52.7°C after adding LiTFSI. The above results revealed that HBPS-(PS-*b*-PPEGMA950)$_{26}$ was a proper material for polymer electrolyte matrix.

Thermal Stability

The thermal stability of the obtained star block polymers was characterized by TGA. Figure 19 shows the TGA curves of the obtained HBPS-(PS-*b*-PPEGMA)$_{26}$. All the star block polymers exhibited good thermal stability, especially for star polymers with the longest PEO side chains. T_{onset} of HBPS-(PS-*b*-PPEGMA950)$_{26}$ was above 370°C and was not greatly influenced by the content of PEO.

Mechanical Properties

For HBPS-(PS-*b*-PPEGMA)$_{26}$ polymer electrolytes with different lengths of PEO chains and similar PEO content of about 60 wt %, flexible freestanding films were prepared by solution-casting technique. These polymer electrolytes had good film-forming properties. Figure 20 shows the photographs of HBPS-(PS-*b*-PPEGMA950)$_{26}$/LiTFSI electrolyte film with PEO content of 69.3 wt % and EO/Li of 20. But when the PEO content was 74.0 wt % for HBPS-(PS-*b*-PPEGMA950)$_{26}$, the SPE films were too tacky to be removed from the substrate. However, polymer electrolytes based on HBPS-(PPEGMA950)$_{26}$ and PPEGMA950 without PS blocks were sticky liquid at 25°C, whereas polymers electrolytes based on HBPS-(PS-*b*-PPEGMA950)$_{26}$ were solid. Therefore, the existence of polystyrene blocks was in favor of improving the mechanical properties. From the above discussion, it was concluded that the prepared star block polymers had good mechanical properties, and meanwhile, kept relatively high ionic conductivity.

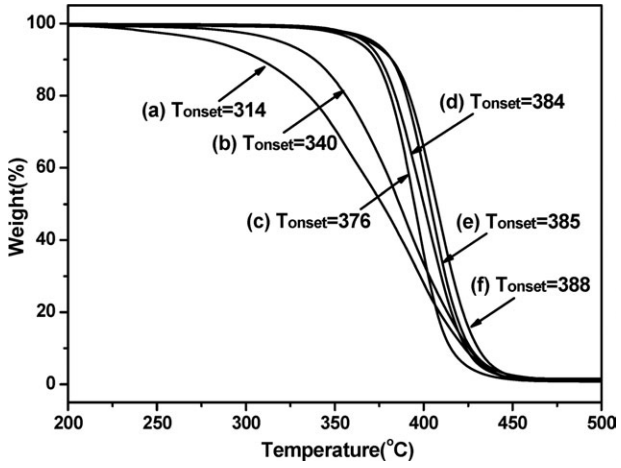

Figure 19. TGA curves of HBPS-(PS-*b*-PPEGMA)$_{26}$ with different PEO side-chain lengths and PEO contents (a) PEGMA300/62.2%, (b) PEGMA475/60.1%, (c) PEGMA950/54.1%, (d) PEGMA950/59.6%, (e) PEGMA950/69.3%, and (f) PEGMA950/74.0%.

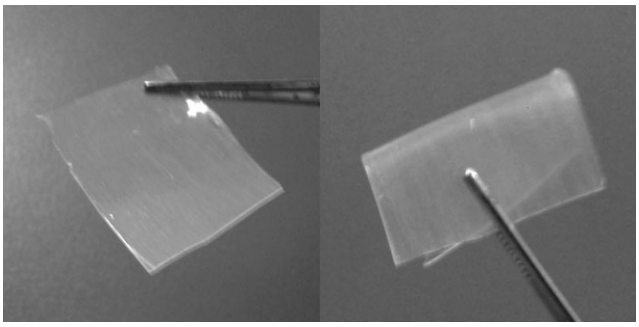

Figure 20. Photographs of HBPS-(PS-*b*-PPEGMA950)$_{26}$/LiTFSI electrolyte film with PEO content of 69.3 wt % and EO/Li of 20.

CONCLUSIONS

A series of multiarm star block polymers HBPS-(PS-*b*-PPEGMA)$_{26}$ with a HBPS core and block arms (PS-*b*-PPEGMA) were successfully synthesized by ATRP. All-solid polymer electrolytes based on these multiarm star polymers were prepared by solution-casting technique. The influences of PEO side-chain length, PEO content, lithium salt concentration and type, and the molecular structure of polymers on the ionic conductivity were systematically studied. The results showed that polymer electrolyte with the longest PEO side chains and the highest PEO content possessed the highest ionic conductivity. The maximum value was 0.8 × 10^{-4} S cm^{-1} at 25°C with EO/Li of 30. The TGA results showed that the thermal stability of the prepared multiarm star block polymers increased with the increase of PEO side-chain length, and HBPS-(PS-*b*-PPEGMA950)$_{26}$ exhibited T_{onset} above 370°C, not greatly affected by the content of PEO. The mechanical property of the star block polymer electrolytes was greatly improved owing to the incorporation of polystyrene blocks, and flexible freestanding films were obtained.

ACKNOWLEDGMENTS

The authors gratefully acknowledge the financial supports provided by the National Natural Science Foundation of China (No. 51073170, 50703044).

REFERENCES

1. Tarascon, J. M.; Armand, M. *Nature* **2001**, *414*, 359.
2. Scrosati, B.; Garche, J. *J. Power Source* **2010**, *195*, 2419.
3. Dias, F. B.; Plomp, L.; Veldhuis, J. B. J. *J. Power Source* **2000**, *88*, 169.
4. Quartarone, E.; Mustarelli, P.; Magistris, A. *Solid State Ionics* **1998**, *110*, 1.
5. Croce, F.; Appetecchi, G. B.; Persi, L.; Scrosati, B. *Nature* **1998**, *394*, 456.
6. Lightfoot, P.; Mehta, M. A.; Bruce, P. G. *Science* **1993**, *262*, 883.
7. Shin, J. H.; Henderson, W. A.; Passerini, S. *J. Electrochem. Soc.* **2005**, *152*, A978.
8. Ramesh, S.; Yuen, T. F.; Shen, C. *J. Spectrochim. Acta Part A* **2008**, *69*, 670.
9. Wu, C. G.; Wu, C. H.; Lu, M. I.; Chuang, H. J. *J. Appl. Polym. Sci.* **2006**, *99*, 1530.
10. Liu, Y.; Lee, J. Y.; Hong, L. *J. Appl. Polym. Sci.* **2003**, *89*, 2815.
11. Egashira, M.; Todo, H.; Yoshimoto, N.; Morita, M. *J. Power Source* **2008**, *178*, 729.
12. Fullerton-Shirey, S. K.; Maranas, J. K. *Macromolecules* **2009**, *42*, 2142.
13. Syzdek, J.; Armand, M.; Marcinek, M.; Zalewska, A.; Żukowska, G.; Wieczorek, W. *Electrochim. Acta* **2010**, *55*, 1314.
14. Ibrahim, S.; Yassin, M. M.; Ahmad, R.; Johan, M. R. *Ionics* **2011**, *17*, 399.
15. Fonseca, C. P.; Neves, S. *J. Power Source* **2002**, *104*, 85.
16. Kim, S. H.; Kim, J. Y.; Kim, H. S.; Cho, H. N. *Solid State Ionics* **1999**, *116*, 63.
17. Vassal, N.; Salmon, E.; Fauvarque, J. F. *Electrochim. Acta* **2000**, *45*, 1527.
18. Ding, L. M.; Shi, J.; Yang, C. Z. *Synthetic Metals* **1997**, *87*, 157.
19. Cho, K. Y.; Lee, K. H.; Park, J. K. *Polym. J.* **2000**, *32*, 537.
20. Bakker, A.; Lindgren, J.; Hermansson, K. *Polymer* **1996**, *37*, 1871.
21. Singh, M.; Odusanya, O.; Wilmes, G. M.; Eitouni, H. B.; Gomez, E. D.; Patel, A. J.; Chen, V. L.; Park, M. J.; Fragouli, P.; Iatrou, H.; Hadjichristidis, N.; Cookson, D.; Balsara, N. P. *Macromolecules* **2007**, *40*, 4578.
22. Bannister, D. J.; Davies, G. R.; Ward, I. M.; Mclntyre, J. E. *Polymer* **1984**, *25*, 1600.
23. Selvaraj, I. I.; Chaklanobis, S.; Manoravi, P.; Chandrasekhar, V. *Polymer* **1995**, *36*, 2603.
24. Chung, J. S.; Sohn, H. J. *J. Power Source* **2002**, *112*, 671.
25. Hawker, C. J.; Chu, F. K.; Pomery, P. J.; Hill, D. J. T. *Macromolecules* **1996**, *29*, 3831.
26. Itoh, T.; Ichikawa, Y.; Hirata, N.; Uno, T.; Kubo, M.; Yamamoto, O. *Solid State Ionics* **2002**, *150*, 337.
27. Lee, S. I.; Schömer, M.; Peng, H. G.; Page, K. A.; Wilms, D.; Frey, H.; Soles, C. L.; Yoon, D. Y. *Chem. Mater.* **2011**, *23*, 2685.
28. Yang, X. H.; Sun, X. Y.; Shao, J. J.; Liu, Y. H.; Wang, X. L. *J. Polym. Sci. Part B: Polym. Phys.* **2004**, *42*, 4195.
29. Marzantowicz, M.; Dygas, J. R.; Krok, F.; Tomaszewska, A.; Florjańczyk, Z.; Zygadło-Monikowska, E.; Lapienis, G. *J. Power Source* **2009**, *194*, 51.
30. Peng, Y.; Liu, H. W.; Zhang, X. Y. *J. Polym. Sci. Part A: Polym. Chem.* **2009**, *47*, 949.
31. Wu, H. Y.; Saikia, D.; Lin, C. P.; Wu, F. S.; Fey, G. T. K.; Kao, H. M. *Polymer* **2010**, *51*, 4351.
32. Niitani, T.; Amaike, M.; Nakano, H.; Dokko, K.; Kanamura, K. *J. Electrochem. Soc.* **2009**, *156*, A577.
33. Peng, Y.; Liu, H. W.; Zhang, X. Y. *J. Polym. Sci. Part A: Polym. Chem.* **2009**, *47*, 949.
34. Zhang, C. H.; Li, J. G.; Zhang, J.; Zhang, L. Y.; Li, H. Y. *Polym. Adv. Technol.* **2010**, *21*, 710.
35. Muñoz-Bonilla, A.; van Herk, A. M.; Heuts, J. P. A. *Macromolecules* **2010**, *43*, 2721.
36. Wang, F. M.; Cheng, J. H.; Hwang, B. J.; Santhanam, R. *J. Solid State Electrochem.* **2012**, *16*, 157.
37. Niitani, T.; Shimada, M.; Kawamura, K.; Kanamura, K. *J. Power Source* **2005**, *146*, 386.
38. Wen, S. J.; Richardson, T. J.; Ghantous, D. I.; Striebel, K. A.; Ross, P. N.; Cairns, E. J. *J. Electroanal. Chem.* **1996**, *408*, 113.
39. Rey, I.; Lasségues, J. C.; Grondin, J.; Servant, L. *Electrochim. Acta* **1998**, *43*, 1505.